Available online at www.sciencedirect.com
ScienceDirect
Surface & Coatings Technology 201 (2006) 1444–1453
SURFACE & COATINGS TECHNOLOGY
www.elsevier.com/locate/surfcoat

Optical emission characteristics of glow discharge in the N_2–H_2–$Sn(CH_3)_4$ and N_2–Ar–$Sn(CH_3)_4$ mixtures

P. Jamroz *, W. Zyrnicki

Institute of Inorganic Chemistry and Metallurgy of Rare Elements, Chemistry Department, Wroclaw University of Technology, Wyb. Wyspianskiego 27, 50-370 Wroclaw, Poland

Received 21 July 2005; accepted in revised form 8 February 2006
Available online 31 March 2006

Abstract

Optical emission spectroscopy (OES) and optical actinometry were used to investigate 100 kHz low-pressure discharge in nitrogen–hydrogen–tetramethyltin and nitrogen–argon–tetramethyltin mixtures. High energy species have been identified in plasma phase. The emission intensities of main species were monitored as a function of plasma composition. The influence of reactive gases on the decomposition of tetramethyltin was investigated and plasma processes were discussed. Glow discharge plasma was characterized by optical temperatures (the electron excitation temperatures of Sn, Ar, H, vibrational temperatures of CN, N_2, N_2^+ and rotational temperature of N_2^+) and by the electron number density. The obtained results revealed a strong deviation of plasma from LTE state for both analyzed mixtures. The X-ray diffraction method was applied to investigate the structure of deposited materials, being solid products of the tetramethyltin decomposition.

Keywords: Plasma diagnostics; Optical emission spectroscopy; Glow discharge; PACVD; X-ray diffraction; Tetramethyltin

1. Introduction

The plasma-assisted chemical vapour deposition (PACVD) or plasma polymerization method was often used for deposition of Sn:C, Sn:N, Sn-doped a-C:H or SnO_2 thin layers (see e.g. [1–6]). These materials are very interesting in the point of electronic (semiconductor, insulator), optical and protective properties [2–4]. Tetramethyltin (TMT: $Sn(CH_3)_4$) was frequently applied as a source of tin in plasma processes [2,4,6], due to its high volatile at the room temperature.

The low-pressure plasma is widely applied in PACVD and plasma polymerization processes. Nevertheless, the low-pressure plasma generated in glow discharges is still far from to be sufficiently understood. Plasma, produced by means of glow discharges is usually not in thermodynamic equilibrium and such a plasma can be characterized by various temperatures (kinetic, rotational, vibrational, electron excitation). Understanding the plasma non-equilibrium phenomena as well as the chemistry and mechanism of PACVD processes require knowledge of concentrations of species and their energy distribution, i.e. temperature as well as electron number density.

Among plasma diagnostics techniques, optical emission spectroscopy (OES) allows an identification of reactive species and gives information on the energetic properties of plasma and on plasma processes. The main advantage of OES comparing to other plasma diagnostics techniques is its non-intrusive character. This technique was often applied to investigate [6–10] and to control PACVD processes [4,10], as well as to determine plasma parameters, i.e. the excitation [8,9,11], vibrational [6,7,9,12] and rotational [6,7,9,12] temperatures. So far, the OES was very rarely employed for investigation of the PACVD system containing of tin-compound.

Arefi-Khonsari et al. [6] studied the $Sn(CH_3)_4$–O_2–Ar discharge by means of OES and measured the OH rotational and N_2 vibrational temperatures. In another work, Robbins et al. [10] examined the $SnCl_4$–O_2 plasma by means of optical emission spectroscopy and actinometry technique. They found that the emission signal of Cl and $SnCl_x$ were correlated with growth and electrical resistivity of SnO_2 thin layers,

* Corresponding author. Tel.: +48 71 3202494; fax: +48 71 3284330.
E-mail address: wieslaw.zyrnicki@pwr.wroc.pl (P. Jamroz).

0257-8972/$ - see front matter © 2006 Elsevier B.V. All rights reserved.
doi:10.1016/j.surfcoat.2006.02.013

respectively. According to the best knowledge of the authors, there has been no report of using OES for investigation of tetramethyltin–nitrogen plasma.

The present study has been undertaken to investigate processes of tetramethyltin decomposition in the N_2–H_2 and N_2–Ar 100 kHz glow discharge by means of optical emission spectroscopy. It has included identification of plasma active species and determination of parameters characterizing plasma, i.e. optical temperatures (electron excitation, vibrational, and rotational) and the electron number density. To complete knowledge on decomposition of tetramethyltin, the XRD method was used to study solid products deposited on electrodes and cold wall of reactor.

2. Experimental procedures

The experiments were carried out in a Pyrex glass circular reactor with two parallel Armco steel electrodes (diameter 22 mm, thickness 2 mm, space between the electrodes 16 mm) and quartz window [9]. The plasma was generated between two electrodes, using a 200-W 100 kHz power supply. The deposition of thin layers by means of 100 kHz plasma was formerly reported by some authors e.g. [13]. The tetramethyltin (99.9% purity, Aldride made), cooled in ice-water bath, was admitted to the stream of gases via Teflon-valve. The plasma chamber was pumped out by using a vacuum mechanical pump. The cryogenic trap (liquid nitrogen), placed in front of vacuum pump, was used to avoid spreading easy volatile by-products come from tetramethyltin. The nitrogen–hydrogen and nitrogen–argon mixtures (containing of 0, 25%, 50%, 75% and 100% of nitrogen) were employed here as reactive gases. The current of discharge, total pressure and flow rate of tetramethyltin were kept constant and were equal: 100 mA, 532 Pa (4 Torr) and 0.004 g min^{-1}, respectively. Emission intensities were measured near the working electrode (2 mm above the cathode). Generally, the area investigated here (i.e. near the cathode/substrate) is considered as a very important in the point of view of plasma processes leading to a formation of thin layers. However, this area differs from other parts of the plasma (especially from a central part) due to non-uniform distribution of electric field. Usually measurements of plasma spectra were reported for a selected cross-section [14]. Plasma radiation was imaged with an achromatic lens (f=80) onto the entrance slit of low- and high-resolution spectral device. The JY Triax 320 monochromator (f=320, holographic grating 1200 grooves mm^{-1}) with Hamamatsu R-928 photomultiplier was employed here for measurements of low-resolution spectra. High-resolution spectra were recorded by means of computerized system consisting of PGS-2 spectrograph with photomultiplier tube (Hamamatsu DH-3). The changes of photomultiplier optical sensitive versus the wavelength were corrected by means of Bentham reference lamp with Protection Engineering certificate.

The structure of deposited materials was investigated by XRD method. The XRD measurements were performed with Philips X-Pert System by using of Cu-Kα radiation line. The scanning region of 2θ was from 5° to 70°. The deposition process time was approximately 3 h.

3. Results and discussion

3.1. Identification of plasma active species

The emission spectra were recorded in the wavelength range between 200 and 850 nm. In the reactive mixtures containing nitrogen, bands of $N_2^+B^2\Sigma_u^+$–$X^2\Sigma_g^+$ and bands of N_2 (belonging to the $C^3\Pi_u$–$B^3\Pi_g$ and $B^3\Pi_g$–$A^3\Sigma_u^+$ system) were observed. Weak lines of N I (at 742.4, 744.2, 746.8, 818.8, and 821.63 nm) and N II (at 500.5, 500.1, 567.9 and 567.6 nm) were also detected in nitrogen-rich plasmas. In all examined mixtures, the NH ($A^3\Pi$–$X^3\Sigma^-$, 0–0) band at 336.0 nm and lines of hydrogen, H_α (at 656.3 nm), H_β (at 486.13 nm) and H_γ (at 434.0 nm), were observed. Additionally, in the mixtures containing argon, numerous lines of argon: Ar I and Ar II were identified in the ranges of 640–780 nm and 450–520 nm, respectively. The introduction of tetramethyltin to nitrogen–hydrogen or nitrogen–argon mixtures led to the appearance of Sn I lines in the range of 220–320 nm (the strongest lines at 235.5, 242.9, 270.2 and 317.5 nm – see Fig. 1a), the CH ($A^2\Delta$–$X^2\Pi$) with headband at 431.4 nm and C I line at 247.3 nm. Molecular bands of CN corresponding to the strong $B^2\Sigma^+$–$X^2\Sigma^+$(Fig. 1b) and weak $A^2\Pi$–$X^2\Sigma$ transitions were also identified in the mixtures containing nitrogen and tetramethyltin. The CN bands were usually observed in the plasma containing hydrocarbon (or carbon) and nitrogen [7,9]. The continuous spectra and emission intensities of species originated from TMT decomposition (e.g. Sn, C) were distinctly higher in the N_2–Ar–TMT mixture in comparison with the N_2–H_2–TMT mixture (Fig. 1a). Emission spectra of Sn^+ have not been detected under experimental conditions, employed here.

3.2. Emission intensity of reactive species – plasma processes

The emission intensities of the species, Sn, H, CH, C, CN, N_2, N_2^+ and additionally Ar, Ar^+, have been chosen to monitor the behavior of active plasma components versus percentage of nitrogen in the N_2–H_2–TMT (Fig. 2) and N_2–Ar–TMT (Fig. 3) mixtures. These species are expected to play an important role in the deposition and growth process of layer. The wavelengths, assignments and threshold energies of examined species are given in Table 1.

The nitrogen concentration increase in the gas mixture led to a growth of the emission intensities of N_2, CN, N_2^+, Sn, C and CH in the N_2–H_2–TMT mixture (Fig. 2). Only the emission of H showed a different dependence on the percentage of nitrogen. Firstly, it increased and then decreased.

For the N_2–Ar–TMT mixture, the intensities of Ar I and Ar II decreased and N_2^+, N_2 and CN increased with the growth of nitrogen contribution in mixture (Fig. 3). The intensities of H and C I are slightly decreased versus the nitrogen fraction in the N_2–Ar–TMT mixture, whereas the emission intensity of CH showed minimum value for N_2/Ar=1/1. The emission intensity

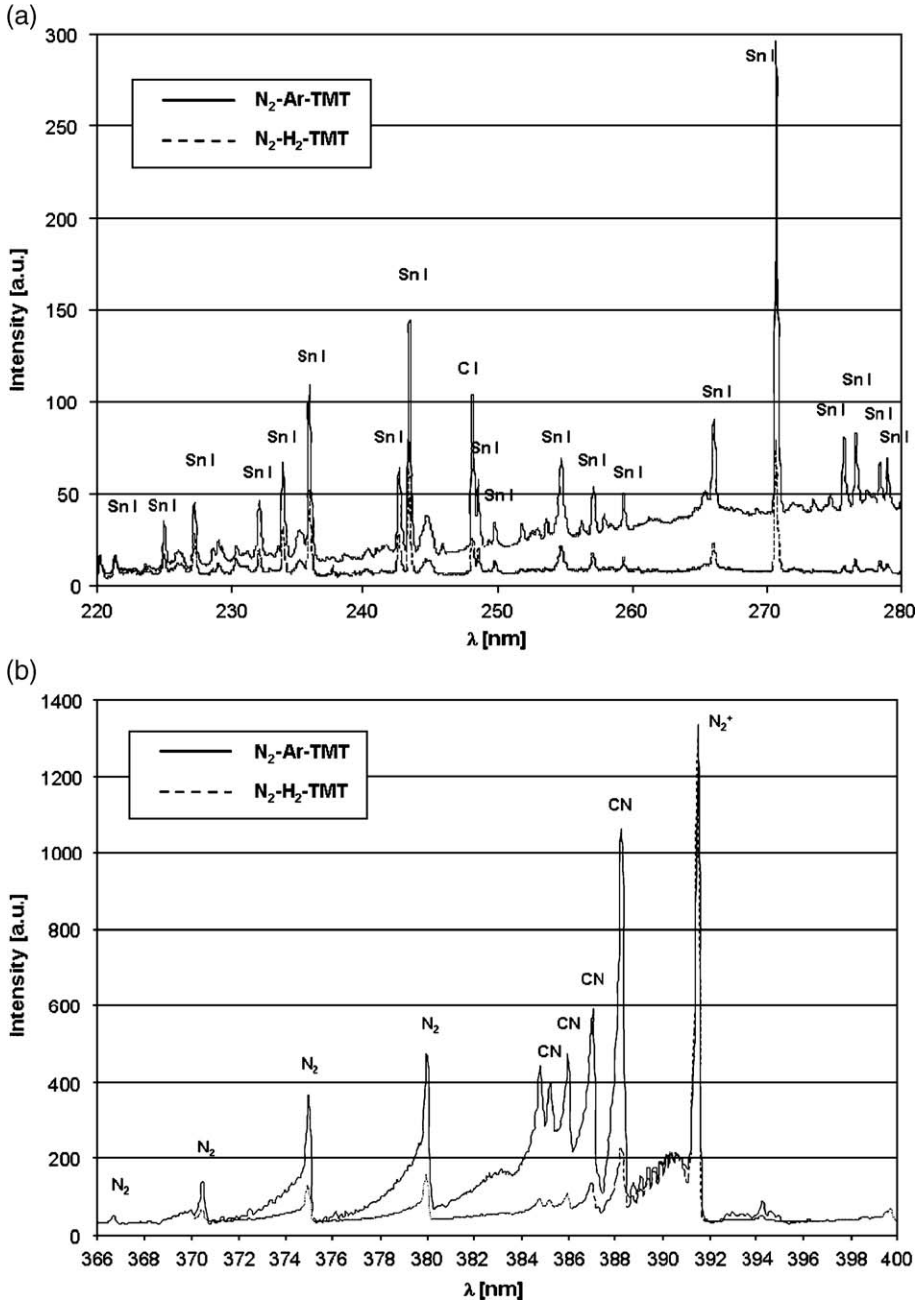

Fig. 1. Optical emission spectra from the N_2–Ar–TMT (solid line) and N_2–H_2–TMT (dotted line) 100 kHz discharge in the range of (a) 220–280 nm and (b) 366–400 nm.

of Sn I drastically decreased firstly to reach a minimum at about 25% of nitrogen and then increased. As can be seen in Fig. 3, the emission intensity of Sn I in the Ar–TMT mixture (0% N_2) is similar to that recorded in the mixture containing 100% N_2 i.e. N_2–TMT.

The experimental results for the CN, N_2 and N_2^+ species in the N_2–H_2–TMT and N_2–Ar–TMT mixtures suggest that the dominant mechanism of excitation for these species must be the same.

Breaking of the Sn–CH_3 bond by, e.g. electron impact, is believed to be a first $Sn(CH_3)_4$ fragmentation step, because the energy of Sn–C bond (297 kJ/mol) is lower than in the C–H bond (420–460 kJ/mol) [15]:

$$Sn(CH_3)_4 + e = Sn(CH)_{4-x} + xCH_3 + e \quad (1)$$

The methyl radical (CH_3) formed via reaction (1) may be dissociated next by direct electron impacts:

$$CH_3 + e = CH(A) + 2H + e \quad (2)$$

$$CH_3 + e = CH_2 + H + e \quad (3)$$

Fragmentation of tetramethyltin and/or other fragments come from TMT, in the mixture containing argon, can

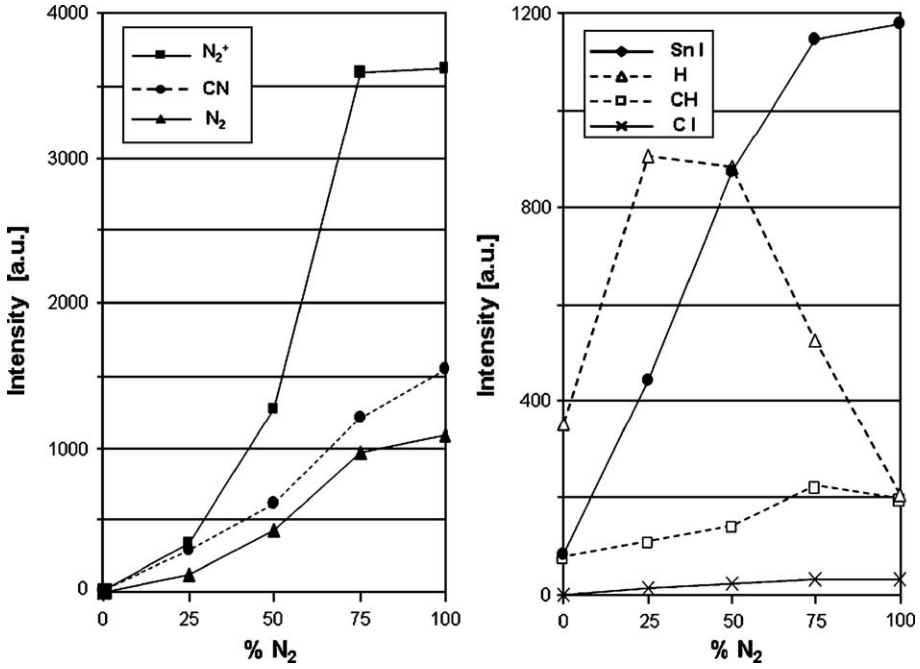

Fig. 2. Emission intensities of N_2^+, CN, N_2, Sn, H, CH and C species versus percentage of nitrogen in the N_2–H_2–TMT mixture.

also be caused by an interaction with high-energy states of argon.

One of the production mechanisms of excited state of CH is electron impact dissociation of CH_3 (reaction (2)). Direct excitation of the ground state of CH molecule, as a result of electron impact, may be neglected, because the CH radicals could react easily and quickly with other species and their concentration in plasma phase is thus very low [16].

Optical actinometry [5,7,17] has been employed here better understand the plasma chemistry in the N_2–H_2–TMT system. For the actinometry technique measurement, a small and constant quantity of argon (~4%) was added to the nitrogen–hydrogen–tetramethyltin mixture. The emission intensities of CN, N_2, H, CH, C and additionally actinometer (Ar) were simultaneously monitored as a function of percentage of nitrogen. Argon (the Ar I line at 750.3 nm) was chosen as

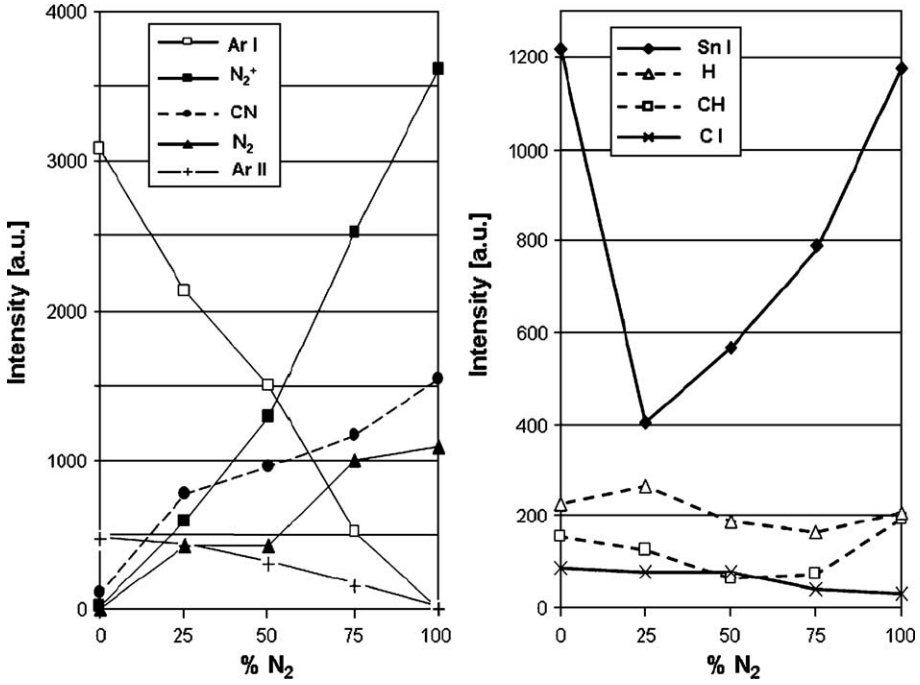

Fig. 3. The variation of the Ar, N_2^+, CN, N_2, Ar^+, Sn, H, CH and C intensities versus the nitrogen percentage in the N_2–Ar–TMT mixture.

Table 1
Spectroscopic data of the measured lines and bands

Species	Wavelength (nm)	Transition	Threshold energy (eV)
Ar	750.39	$2p_1–1s_2$	13.48
Ar^+	487.98	$3p^4(^3P)\ 4p–3p^4(^3P)\ 4s$	19.68
C	247.86	$3s^1\ (P^o)–2p^2\ (^1S)$	7.68
H	656.28	$3d\ (^2D)–2p\ (^2P^o)$	12.08
Sn	317.51	$6s\ (^3P)–5p\ (^3P)$	4.3
CH	431.40	$(0–0)\ A^2\Delta–X^2\Pi$	2.88; ~11 [a]
CN	388.43	$(0–0)\ B^2\Sigma–X^2\Sigma$	3.2
N_2	380.49	$(0–2)\ C^3\Pi_u–B^3\Pi_g$	11.2
N_2^+	391.44	$(0–0)\ B^2\Sigma_u^+–X^2\Sigma_g^+$	18.7

[a] Value reported in [18].

actinometer, because its excitation energy is quite close to the threshold energy of H, N_2 and CH (see Table 1). The energy of the upper electronic state of CN and C is meaningfully differed to the excitation energy of actinometer. Nevertheless, based on earlier works [7,17,18], the optical actinometry was also applied to determine the CN and C relative concentrations.

The evolution of the CN, N_2, H, CH and C relative concentrations, deduced from the variation of the intensity ratios: I(CN)/I(Ar), I(N_2)/I(Ar), I(H)/I(Ar), I(CH)/I(Ar) and I(C)/I(Ar) is presented in Fig. 4 for the N_2–H_2–TMT mixture. The concentrations of CN and N_2 species increase in a similar manner compared with the nitrogen fraction in the mixture. It may be indicated that nitrogen plays an important role in the production of CN molecules. The linear drop of the H concentration with a decrease of hydrogen contribution may suggest that the H atoms are mainly produced by the dissociation of the H_2 molecules. In the range of nitrogen concentration from 25% to 100%, the CH concentration was practically independent of the gas composition. The growth of CH concentration was observed only for the H_2–TMT mixture, where the H atoms were probably responsible for the enhanced production of hydrocarbon fragments. The change in nitrogen percentage had little influence on the I(C)/I(Ar) ratio.

3.3. Plasma temperatures and electron number density

Knowledge of plasma temperatures (electron excitation, vibrational, rotational) and quantity of "free electrons", i.e. electron number density, are crucial for understanding the non-equilibrium phenomena and the excitation mechanism occurring in the discharge.

The electron excitation temperature (T_{exc}), described by the relatively excited level population, is an important parameter for the characterization of plasma. The excitation temperatures of Ar I and Sn I were obtained by a Boltzmann plot according to the follow equation, assuming a partial local thermal equilibrium state (p-LTE) [1]:

$$\ln\left(I_{em}^{nm}\lambda_{nm}/g_nA_{nm}\right) = C - E_n/kT_{exc} \quad (4)$$

where: I_{em} – the line intensity, λ – wavelength of light emitted species, g – statistical weight, A – transition probability, E – energy of the upper levels, k – Boltzmann constant, C – constant, n and m denote the upper and lower states.

Eight lines of Sn I (at 231.72, 233.48, 235.48, 242.95, 284.00, 285.06, 300.91, and 317.51 nm) and nine lines of Ar I, so-called "red", (at 675.28, 687.13, 696.54, 703.03, 706.72, 714.70, 720.70, 727.29, and 737.21 nm) were applied here for determination of the electron excitation temperatures. Plotting $\ln(I\lambda/gA)$ against E yields a straight line with a slope equal to $-1/kT_{exc}$. The uncertainty in determining the slope of the regression line can be used for estimating error. Two-line

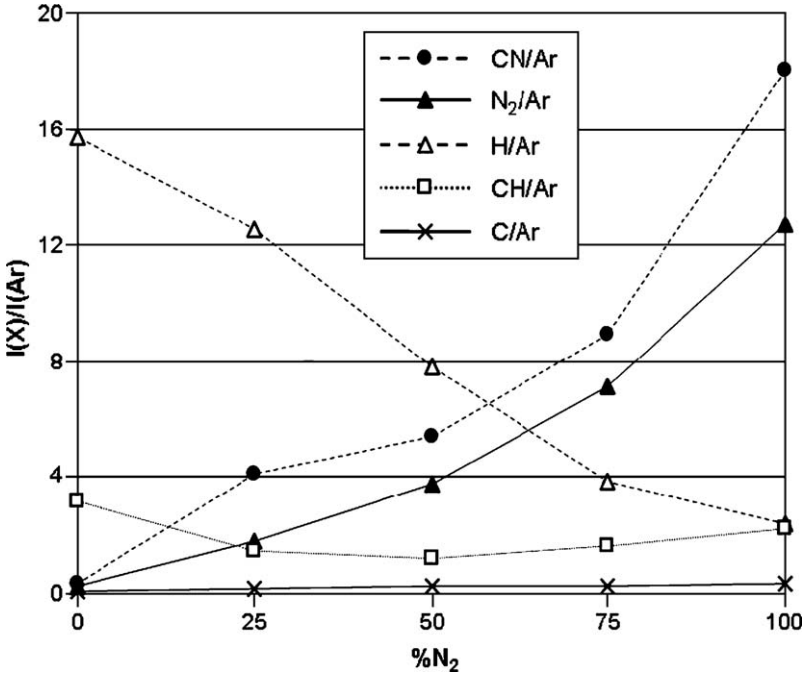

Fig. 4. Relative concentrations of CN, N_2, H, CH and C species as a function of nitrogen percentage in the N_2–H_2–TMT mixture.

radiance ratio method [1] was used to determine the H excitation temperature. Two hydrogen lines: H_α (at 656.28 nm) and H_β (at 486.13 nm) were employed here. The spectroscopic data of Ar, Sn and H, i.e. transition probabilities, statistical weights and energies of the upper levels were obtained from NIST Atomic Spectra Database [19]. The uncertainties for the measurement of excitation temperatures were 10–15%. Boltzmann plots for the Ar I and Sn I lines were presented in Fig. 5. The distribution of emission intensity of Sn I and Ar I lines are described by the Boltzmann law.

The relation between the vibrational band intensity (I_{em}) and vibrational temperature (T_{vib}) can be written as follows [1]:

$$\ln\left(\frac{I_{em}^{v'v''}}{q_{v'v''}\nu_{v'v''}^4}\right) = C_1 - \frac{G(v)}{kT_{vib}} \quad (5)$$

where: $q_{v'v''}$ – the Franck–Condon factor, ν – the transition frequency, $G(v')$ – the vibrational energy of the upper state, v – vibrational quantum number.

The vibrational temperatures (T_{vib}) of N_2, CN and N_2^+ were calculated from relation (5) using the (3–3), (2–2), (1–1), and (0–0) bands of the $B^2\Sigma$–$X^2\Sigma$ of CN system, six bands of N_2 $C^3\Pi_u$–$B^3\Pi_g$, the transition, i.e. (3–2), (2–1), (1–0), (2–4), (1–3), (0–2) and two bands of $N_2^+B^2\Sigma_u^+$–$X^2\Sigma_g^+$, (1–2) and (0–1). The molecular constants and Franck–Condon factors have been taken from Jamroz and Zyrnicki [7] and Herzberg [20].

The rotational temperature (T_{rot}) was determined by the Boltzmann plot method employing the R(4)–R(21) rotational lines of the $N_2^+B^2\Sigma_u^+$–$X^2\Sigma_g^+$ (0–0) band, from the relation [1]:

$$\ln\left(\frac{I_{em}^{K'K''}}{K'+K''+l}\right) = C_2 - \frac{F_v(K')}{kT_{rot}} \quad (6)$$

where: I_{em} – the rotational line intensity, $F(K')$ – the energy of the upper rotational state, K', K'' – the rotational quantum numbers of the upper and lower states, C_2 – constant.

The other details have been presented in an earlier work [7]. The standard deviation uncertainties (ΔT) for the vibrational and rotational temperatures were 10–15% and 2–5%, respectively.

The Stark broadening of the H_β line served to estimate the electron number density. The full width at half maximum (FWHM) of the hydrogen line due to Stark effect ($\Delta\lambda_{1/2}$) in Å is related to electron number density (N_e), according to Griem theory [21]: $N_e = C(N_e, T_e) * (\Delta\lambda_{1/2})^{3/2}$, where: $C(N_e, T_e) = 3.58 \times 10^{14}\,\text{Å}^{-3/2}\,\text{cm}^{-3}$ – constant.

The profiles of the hydrogen line were measured in the second order by means of the high-resolution spectrograph. The experimental profiles of H_β line were fitted with Lorentz profile. The calculated FWHM of line was corrected for the instrumental and Doppler broadening of the line (~0.03 nm). A relative standard deviation uncertainty of electron density was determined to be below 20%.

Changes of the excitation, vibrational and rotational temperatures versus plasma gas composition (percentage of nitrogen in the mixture) were investigated. Fig. 6 illustrates the excitation temperatures of Ar I, H and Sn I as a function of the percentage of nitrogen in the N_2–H_2–TMT and N_2–Ar–TMT mixtures. The excitation temperatures of H and Sn I in the N_2–H_2–TMT plasma (Fig. 6a) were nearly equal and increased from 5200 K to 8000 K with the growth of nitrogen percentage. In the N_2–Ar–$Sn(CH_3)_4$ discharge, in the above described N_2–H_2–TMT system, the excitation temperatures were differed considerably (Fig. 6b). Nevertheless, the values of the Ar I and H excitation temperature in N_2–Ar–TMT plasma are consistent with those reported for low-pressure ICP [8] and rf plasma [11], respectively. The excitation temperatures of Ar I, H and Sn I in the nitrogen–argon–tetramethyltin system were varied from 9500 K to 12 000 K, from 8000 K to 8700 K and from 5300 K to 8000 K, respectively.

The variations of the vibrational temperatures of CN, N_2 and N_2^+ as a function of nitrogen percentage are shown in Fig.

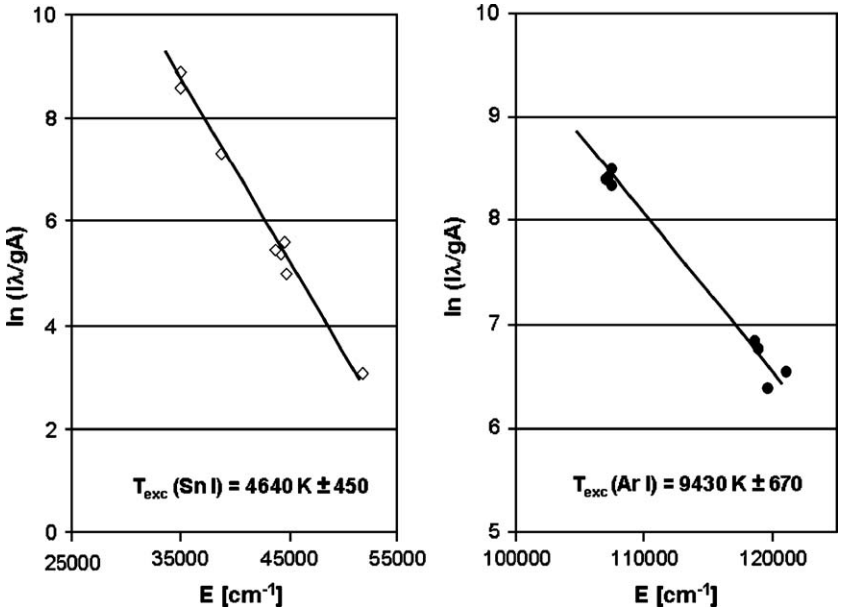

Fig. 5. The Boltzmann plots for Sn I and Ar I lines.

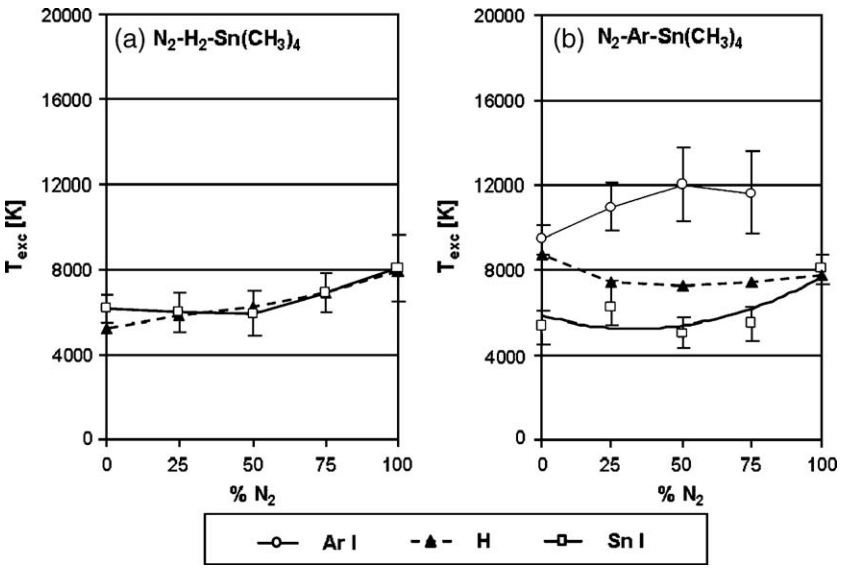

Fig. 6. The excitation temperatures of Ar I, H and Sn I in the (a) N_2–H_2–TMT and (b) N_2–Ar–TMT mixtures.

7. In both mixtures, the growth of nitrogen percentage caused a decrease in the vibrational temperature of CN. The T_{vib}(CN) varied from 4350 K to 7400 K and from 3850 K to 5200 K in the N_2–H_2–TMT and N_2–Ar–TMT discharge, respectively. In the N_2–H_2–TMT and N_2–Ar–TMT glow discharges, the vibrational temperatures of N_2 and N_2^+ were 2750–2900 K and 1500–1750 K, respectively. The $T_{vib}(N_2)$ and $T_{vib}(N_2^+)$ values were almost independent on the nitrogen concentration in the source gas. As can be seen in Fig. 7, the highest value of vibrational temperature was observed for the CN molecule, while the N_2 and N_2^+ vibrational temperatures were considerably lower. On possible reason for the differences between the vibrational temperatures of CN, N_2 and N_2^+ in the examined mixtures is that species are produced as a results of various mechanisms. The excitation states of N_2 and N_2^+ are probably populated by electron impact, whereas the CN molecule may be formed (at least partially) as a result of impact of high-energy species (e.g. hydrocarbon with active nitrogen).

Table 2 shows the rotational temperatures of N_2^+ for the N_2–H_2 and N_2–Ar mixtures with and without tin–organic compound i.e. $Sn(CH_3)_4$. Values of the rotational temperature are comparable to the plasma gas temperature, i.e. kinetic temperature [7]. Based on the previous works [22], the rotational temperatures of N_2^+ presented here can be considered as electrode temperature. The introduction of tetramethyltin to the nitrogen–hydrogen or nitrogen–argon mixture did not cause significant changes of the rotational temperature of N_2^+ as can be seen in the Table 2. For the N_2–H_2–$Sn(CH_3)_4$ discharge, the N_2^+ rotational temperature was dependent on plasma gas

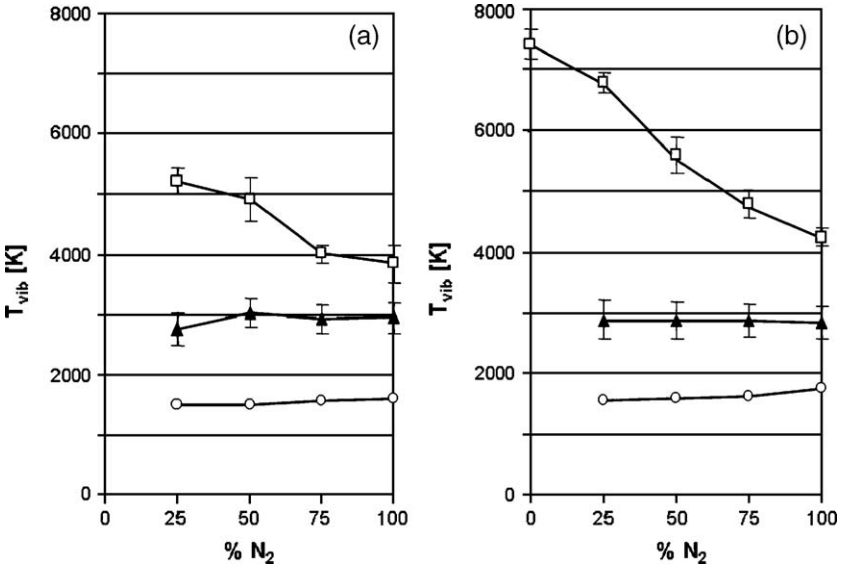

Fig. 7. The vibrational temperatures of the CN (□), N_2 (△) and N_2^+ (○) versus percentage of nitrogen in the (a) N_2–H_2–TMT and (b) N_2–Ar–TMT mixtures.

Table 2
The influence of addition of tetramethyltin to the N_2–H_2 and N_2–Ar mixtures on the rotational temperature of N_2^+

% N_2	N_2–H_2 $T_{rot}\pm\Delta T$ (K)	N_2–H_2–$Sn(CH_3)_4$ $T_{rot}\pm\Delta T$ (K)	N_2–Ar $T_{rot}\pm\Delta T$ (K)	N_2–Ar–$Sn(CH_3)_4$ $T_{rot}\pm\Delta T$ (K)
25	534±15	490±22	792±31	795±35
50	662±18	607±25	738±22	755±25
75	670±20	740±19	755±14	742±19
100	783±15	775±21	784±15	775±20

composition and ranged from 490 K to 775 K, while for the N_2–Ar–$Sn(CH_3)_4$ mixture the temperature was approximately constant (740 K–795 K). The N_2 vibrational and rotational temperatures measured here for the N_2–H_2–TMT and N_2–Ar–TMT discharges are slightly higher, but comparable with those reported for the O_2–Ar–$Sn(CH_3)_4$ plasma [6] and for the system containing nitrogen and tetramethylsilane [9].

Finally, in the both N_2–Ar–TMT and N_2–H_2–TMT discharges, the following relation between the excitation, vibrational and rotational temperatures has been observed:

$$T_{exc}(Ar) > T_{exc}(H) \geq T_{exc}(Sn) \geq T_{vib}(CN) >> T_{vib}(N_2) > T_{vib}(N_2^+) > T_{rot}(N_2^+)$$

The great differences between the temperatures (excitational, vibrational and rotational) indicate that N_2–H_2–TMT and N_2–Ar–TMT low-pressure 100 kHz plasma was in a non-equilibrium state.

The estimated electron density number (N_e) vs. percentage of nitrogen for both nitrogen–hydrogen and nitrogen–argon mixture discharges is presented in Fig. 8. The N_e values in the nitrogen–hydrogen discharge increased rapidly with the N_2 contribution, while in the nitrogen–argon atmosphere, N_e showed a small growth. A similar behavior of electron density versus nitrogen percentage has been noted for plasma containing tin organic compound, i.e. tetramethyltin. Addition of TMT to the nitrogen–hydrogen or nitrogen–argon mixtures caused a significant decrease in electron number density. This is a consequence of dissociation effect of $Sn(CH_3)_4$, where electrons are responsible for breaking chemical bonds and for other processes leading to the formation of active species. Similar to the electron density, the behavior of the intensity ratios of N_2^+/N_2 and Ar^+/Ar increased vs. the N_2 contribution in the analyzed mixtures. The electron number density values (N_e) found here are much higher than measured e.g. by means of Langmuir probe. However, on the other side, these N_e values are in a good agreement with data for low-pressure glow discharges [23].

3.4. XRD study of deposited materials

Both in N_2–H_2–TMT and N_2–Ar–TMT 100 kHz discharges, solids of silver–grey black color were deposited on the working electrode (cathode) and on cold walls of the reactor. For the examination of the deposited materials, the X-ray diffractometry method was employed. Fig. 9a and b show the XRD patterns of the materials originated from TMT–N_2–H_2 and TMT–N_2–Ar discharges, respectively. Sharp peaks due to crystalline phase as well as amorphous spectra with very broad diffuse structure were observed in the diffraction patterns. The identification of the crystalline phase was carried out by means of JCPDS database. The peaks observed in the pattern are associated with the Sn metallic crystalline phase. Similar peaks due to tin crystalline phase were noticed Inoue and co-workers [2] in the thin films deposited from CH_4–H_2–$Sn(CH_3)_4$ mixture. No peaks corresponding to other crystalline phases of tin–compounds (e.g. SnO_2) were noticed here and neither previously [2]. Intensities of the diffraction peaks were higher in

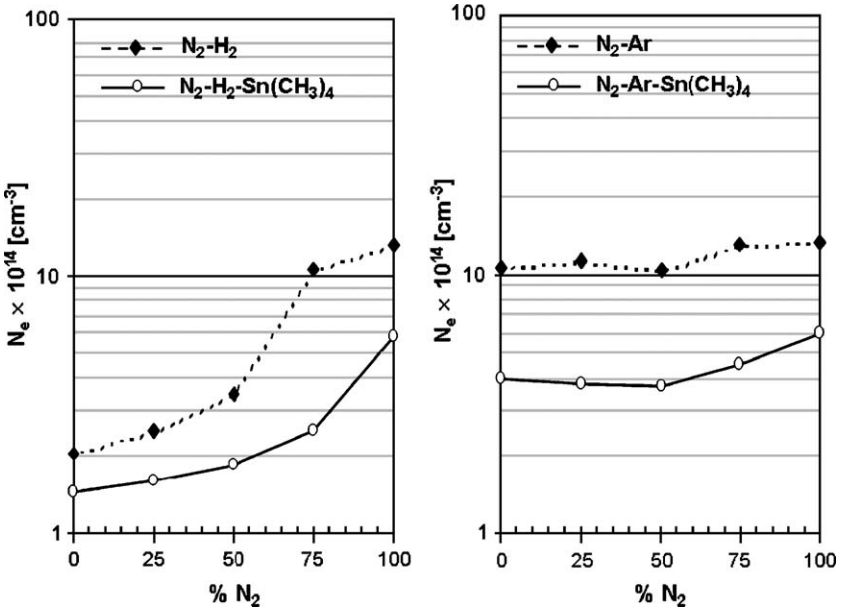

Fig. 8. Electron number density in the (a) N_2–H_2 and (b) N_2–Ar mixtures without (dotted line) and with (solid line) tetramethyltin.

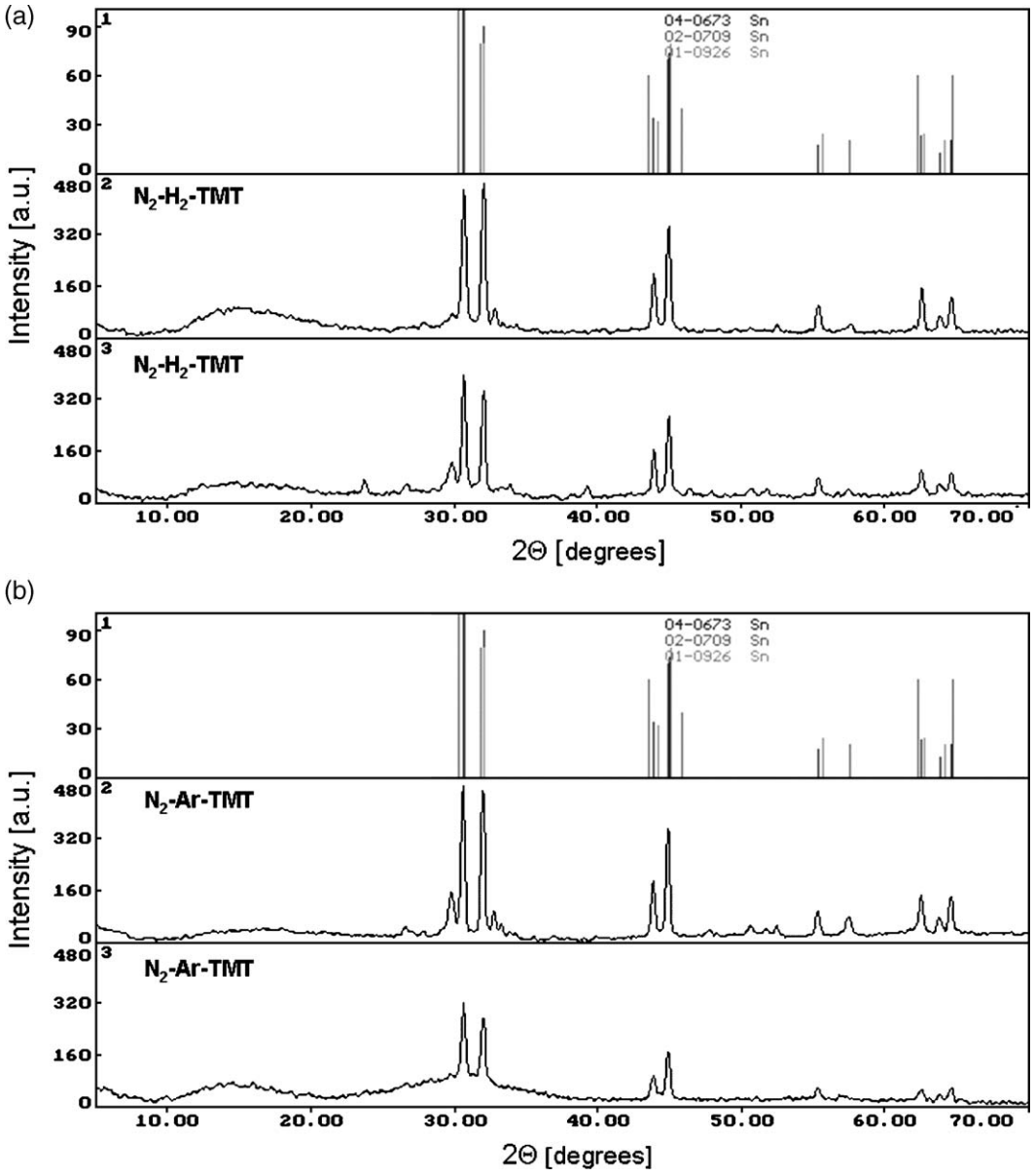

Fig. 9. XRD pattern obtained from deposited materials for the (a) N_2–H_2–TMT ($N_2/H_2 = 1/1$) and (b) N_2–Ar–TMT ($N_2/Ar = 1/1$) mixtures. (1) Diffraction peaks of Sn from JCPDS database; (2) material deposited on working electrode (cathode); (3) material collected from the wall of the chamber.

the materials deposited on the electrode in comparison to these collected from the reactor wall.

4. Conclusions

The decomposition of tetramethyltin in the N_2–H_2 and N_2–Ar discharges has been studied here by optical emission spectroscopy method for the first time. Concentration of species in excited states and in their ground states depended clearly on the gas mixture composition. Replacement of hydrogen by argon led to higher emission intensities of C and H species.

The relation between the electron excitation, vibrational and rotational temperatures: $T_{exc} > T_{vib} > T_{rot}$ indicated that plasma generated in the N_2–H_2–TMT and N_2–Ar–TMT mixtures is not in an equilibrium state. The CN vibrational temperature was found to be sensitive to the nitrogen concentration in the discharge. Lowering of the electron density number due to the introduction of TMT suggests that the decomposition of tetramethyltin by electron impact is the dominating process both in the N_2–H_2–TMT and in the N_2–Ar–TMT mixtures.

The Sn metallic crystalline phases, as well as amorphous phases, have been detected in the layers deposited on the electrode and on the materials collected from the cold wall of the reactor.

References

[1] M. Konuma, Film Deposition by Plasma Techniques, Springer Verlag, Berlin Heidelberg, 1992.
[2] Y. Inoue, T. Komoguchi, H. Nakata, O. Takai, Thin Solid Films 322 (1998) 41.
[3] J. Tyczkowski, B. Pietrzyk, Y. Hatanaka, Y. Nakanishi, Appl. Surf. Sci. 113–114 (1997) 534.

[4] J. Hu, Y. Zong, Yu-Zhong Wang, R. Forch, W. Knoll, Thin Solid Films 472 (2005) 58.
[5] O. Keles, G. Aykac, O.T. Inal, Surf. Coat. Technol. 172 (2003) 166.
[6] F. Arefi-Khonsari, N. Bauduin, F. Donsanti, J. Amouroux, Thin Solid Films 427 (2003) 208.
[7] P. Jamroz, W. Zyrnicki, Eur. Phys. J. Appl. Phys. 19 (2002) 201.
[8] A. Okada, K. Kijima, Vacuum 65 (2002) 319.
[9] P. Jamroz, W. Zyrnicki, Diamond Relat. Mater. 14 (2005) 1498.
[10] J.J. Robins, R.T. Alexander, W. Xiao, T.L. Vincent, C.A. Wolden, Thin Solid Films 406 (2002) 145.
[11] J.L. Jauberteau, I. Jauberteau, J. Aubreton, J. Phys., D, Appl. Phys. 35 (2002) 665.
[12] S. Maeda, H. Matsuo, K. Kuwahara, Y. Matsuda, H. Kuwahara, H. Fujiyama, Surf. Coat. Technol. 97 (1997) 404.
[13] M.C. Kim, J.G. Han, S.B. Lee, J.H. Boo, Surf. Coat. Technol. 169–170 (2003) 281.
[14] S. Peter, H. Giegengack, F. Richter, R. Tabersky, U. Konig, Thin Solid Films 398–399 (2001) 343.
[15] D.R. Linde (Ed.), Handbook of Chemistry and Physics, 75th Ed., CRC Press, Boca Raton, 1994.
[16] P. Cappezuto, G. Bruno, Pure Appl. Chem. 60 (1988) 633.
[17] P. Favia, M. Creatore, F. Palumbo, V. Colaprico, R. d'Agostino, Surf. Coat. Technol. 142–144 (2001) 1.
[18] S.F. Durrant, N. Marcal, S.G. Castro, R.C.G. Vinhas, M.A. Bica de Moraes, J.H. Nicola, Thin Solid Films 259 (1995) 139.
[19] NIST Atomic Spectra Database, http://physics.nist.gov/PhysRefData/ASD/index.html.
[20] G. Herzberg, Molecular spectra and molecular structure, Spectra of Diatomic Molecules, vol. I, D. Van Nostrand Company Inc., New York, 1957.
[21] H.R. Griem, Plasma Spectroscopy, McGraw-Hill, New York, 1964.
[22] A. Brant, J.L.R. Muzart, A.R. de Souza, J. Phys., D, Appl. Phys. 23 (1990) 1334.
[23] B.W. Acon, Ch. Stehle, H. Zhang, A. Montase, Spectrochim. Acta, B 56 (2001) 527.